Published in IEEE Microwave Theory and Techniques,
Vol 63(10), pp 3081 - 3093 September 2015

A Nodal Continuous-Discontinuous Galerkin Time-Domain Method for Maxwell's Equations

Luis Diaz Angulo, Jesus Alvarez, *Member, IEEE*, Fernando L. Teixeira, *Senior Member, IEEE*, M. Fernández Pantoja, *Senior Member, IEEE*, and Salvador G. Garcia, *Senior Member, IEEE*

***Abstract*—A new nodal hybrid continuous-discontinuous Galerkin time-domain (CDGTD) method for the solution of Maxwell's curl equations is proposed and analyzed. This hybridization is made by clustering small collections of elements with a continuous Galerkin (CG) formalism. These clusters exchange information with their exterior through a discontinuous Galerkin (DG) numerical flux. This scheme shows reduced numerical dispersion error with respect to classical DG formulations for certain orders and numbers of clustered elements. The spectral radius of the clustered semi-discretized operator is smaller than its DG counterpart allowing for larger time steps in explicit time integrators. Additionally, the continuity across the element boundaries allows us a reduction of the number of degrees of freedom of up to about 80% for a low-order three-dimensional implementation.**

***Index Terms*—Continuous-discontinuous Galerkin time-domain (CDGTD), continuous Galerkin (CG) method, discontinuous Galerkin (DG) method, discontinuous Galerkin time-domain (DGTD), Maxwell's equations.**

I. Introduction

GALERKIN finite-element (FEM) techniques are a very flexible class of numerical methods to solve partial differential equations (PDEs). For electromagnetic problems in linear media, they can be implemented either in the frequency domain (FD) or in the time domain (TD). Continuous Galerkin (CG) [1], [2] formulations are more prevalent in FD, either in nodal [3], [4] or in vector formulations [5]–[7], though they can also be found in TD [8]. However, discontinuous Galerkin (DG) formulations are most often found in TD, also either in nodal [9] or in vector forms [10]. However, the most popular approach is to evolve the semi-discrete spatial equations by means of explicit time-integration schemes such as the second-order leap-frog (LF2) [11]–[14] or the fourth-order low-storage explicit Runge–Kutta (LSERK4) [9], [15]–[18]. The maximum time step allowed for stability by these schemes is constrained by the spectral radius of the spatial operator, which in turns depend on the inverse square of the polynomial order P and on the minimum edge length h used for the spatial discretization. This makes the use of p-refinement in DGTD, not common beyond intermediate-orders of $3\sim5$ [14], [19], [20], though higher order implementations are reported to be more parallelizable in GPU-based machines [21]. The use of h-refinement in DGTD, also becomes problematic in multiscale problems, since (local) smaller elements enforce reduced (global) time-steps to ensure stability. Strategies to mitigate this exist, like local time-stepping techniques [12], [14], [15], and implicit-explicit (IMEX) time-integration schemes [22], [23]. Reduction on the spectral radius has been achieved using co-volume filtering [24] and mapping techniques [25], though these are effective only for higher orders. Reduction of algebraic complexity and degrees of freedom (DOFs) has also been addressed by multi-element approaches exploiting the advantages of, mainly, tetrahedral and hexahedral mesh elements. In three-dimensional (3-D) problems this forces the use of nonconforming interfaces [26], [27] or the use of pyramidal elements [28], for the transitions between elements of different types.

CGTD schemes present also interesting features. CG methods use significantly fewer DOFs than DG methods do. They do not introduce dissipation if a symplectic time integrator, such as LF2, is used. Moreover, the spectral radius of the assembled system is smaller than when a DG formalism is used [29], thus allowing the use of larger time-steps.

In this work, we explore the topic of the hybridization of CG and DG schemes. This topic is present in the context of elliptic problems arising to a family of methods known as Mortar methods [30]–[35], hybridizing mixed finite-element (MFE) or HDG methods in different regions of the mesh that have certain homogeneity, while the DG method is used to handle discontinuities on the material properties or at nonconforming interfaces. Among some other benefits, the resulting methods achieve a reduction of DOF and offer the possibility of using a model reduction in different regions. For nonelectromagnetic problems, another approach was explored in [36] and [37] to approximate the shallow water equations using DG for the primitive continuity equation and CG for the momentum equation.

In this paper, we present a new nodal hybrid continuous-discontinuous Galerkin (CDG) method for the solution of the time-domain first-order coupled Maxwell's curl equations. The

Manuscript received September 09, 2014; revised December 28, 2014 and May 15, 2015; accepted July 20, 2015. Date of publication September 17, 2015; date of current version October 02, 2015. This work was supported in part by the National Projects under Grant TEC2010-20841-C04-04, Grant TEC2013-48414-C3-1-R, Grant CSD2008-00068, Grant P09-TIC-5327, and Grant P12-TIC-1442, the GENIL Excellence Network, and the National Science Foundation under Grant ECCE-1305838.

L. D. Angulo, M. F. Pantoja, and S. G. Garcia are with the Department of Electromagnetism, University of Granada, 18071 Granada, Spain (e-mail: lmdiazangulo@ugr.es).

J. Alvarez is with Airbus Defense and Space, 28906 Getafe, Spain.

F. L. Teixeira is with the ElectroScience Laboratory and the Department of Electrical and Computer Engineering, The Ohio State University, Columbus, OH 43212 USA.

Color versions of one or more of the figures in this paper are available online at http://ieeexplore.ieee.org.

Digital Object Identifier 10.1109/TMTT.2015.2472411

proposed method is aimed at taking advantage of a reduced number of DOF and smaller spectral radius in CG while benefiting from the spurious-free and block-diagonal properties of DG. Previous attempts exist [38], employing a two-dimensional (2-D) multi-element hybrid continuous–discontinuous scheme: CG in a structured grid of square elements, and DG in a unstructured triangular grid. In our approach, rather than applying a CG formalism over large regions, we apply it only on small clusters of elements, thus maintaining the easily invertible block-diagonal nature of the global system of linear equations. Thus resulting in an important difference in terms of computational cost. Although we will focus on a nodal CG method, a similar approach could be followed with HDG techniques and for other hyperbolic problems. Thus, an added value of the methodology described in this paper, is to show a possible way of taking profit of other implicit techniques that, due to their computational efficiency, cannot be effectively used in TD. Consequently, this work can potentially be an initial step to connect two branches of numerical methods: spatially implicit and explicit methods.

The remainder of this paper is organized as follows. In Section II, we will briefly revisit the classical nodal CG and DG methods. Next, we will introduce the proposed CDG method and present a numerical study of its numerical-dispersion properties and spectral characteristics in one dimension. Next, a numerical test-case consisting in a 2-D PEC cavity serves to further analyze its spectral properties and to provide a L^2-norm analysis of its h-convergence, for different numerical fluxes and spatial basis orders. We will show an analysis of the computational costs of this technique. Finally, we will present some conclusions from this study and provide an assessment of its benefits in different scenarios.

II. Nodal Galerkin TD Formulations for Maxwell Equations

Maxwell's curl equations in sourceless and homogeneous lossless media are

$$\begin{aligned}\vec{\nabla}\times\vec{E} &= -\mu\partial_t\vec{H}\\ \vec{\nabla}\times\vec{H} &= \varepsilon\partial_t\vec{E}\end{aligned} \tag{1}$$

where $\vec{E}$, $\vec{H}$, ε, μ are, respectively: the electric field, magnetic field, permittivity, and permeability. For simplicity, we will assume that ε and μ do not vary in the computational domain Ω and use a system of units where $\varepsilon = \mu = 1$. A lossy media formulation can be straightforwardly derived [39].

Let us begin our discussion by briefly recalling the fundamentals of the continuous (CG) and discontinuous (DG) Galerkin techniques that can be used to solve (1). Both approaches start by tessellating the computational domain with $k = 1, \ldots, K$ nonoverlapping elements. On each of these elements, the solution is approximated by a projection of the analytical solution onto a finite expansion basis of functions. In this work we will use classical Lagrange interpolation polynomials, i.e., a nodal basis such as the one described in [1]. The Galerkin problem consists of nullifying the inner product of the approximated fields with respect to the same basis of functions, leading to a system of linear equations [29]. However, CG and DG approaches differ since the first one imposes continuity directly on the fields while the second imposes it on a different quantity so-called numerical flux. Once the spatial semi-discretization has been obtained, either scheme can be evolved using a time integration technique. As mentioned before, the two most popular are the LF2 and LSERK4 schemes [15]. In brief, LSERK4 has a higher accuracy at the expense of a higher computational cost than LF2. LSERK4 also introduces some numerical dissipation while the LF2 scheme is symplectic.

A. Continuous Galerkin

The CG formulation imposes the continuity of the fields across element interfaces [1], [29]. This can be expressed succinctly in matrix form as

$$\begin{aligned}\mathcal{Z}\mathcal{M}\mathcal{Z}^T\partial_t\mathbf{E}_g(t) + \mathcal{Z}\mathcal{S}\mathcal{Z}^T\mathbf{H}_g(t) &= 0\\ \mathcal{Z}\mathcal{M}\mathcal{Z}^T\partial_t\mathbf{H}_g(t) - \mathcal{Z}\mathcal{S}\mathcal{Z}^T\mathbf{E}_g(t) &= 0\end{aligned} \tag{2}$$

where $\mathcal{M}$ is the mass matrix and $\mathcal{S}$ is the stiffness matrix, both built independently for each element and assembled together using an operator that we will denote by $\mathcal{Z}$ that collapses each pair of associated nodes on the element boundaries into a single one. $\mathbf{E}_g$ and $\mathbf{H}_g$ are column vectors containing all the degrees of freedom in the computational domain for the electric and magnetic fields, respectively.

B. Discontinuous Galerkin

DG formalism introduces the concept of numerical fluxes as the quantity for which continuity is enforced across element interfaces [40], rather than the fields themselves [9]. Applying this concept, we obtain the following system of equations for each element k:

$$\begin{aligned}\mathcal{M}_k\partial_t\mathbf{E}_k(t) + \mathcal{S}_k\mathbf{H}_k(t) - \sum_f^{N_f}\mathcal{F}_{kf}\mathbf{H}^*_{kf}(t) &= 0\\ \mathcal{M}_k\partial_t\mathbf{H}_k(t) - \mathcal{S}_k\mathbf{E}_k(t) + \sum_f^{N_f}\mathcal{F}_{kf}\mathbf{E}^*_{kf}(t) &= 0\end{aligned} \tag{3}$$

where $\mathcal{F}_{kf}$ is the lift operator [9] for face f and vectors $\mathbf{E}^*_{kf}$ and $\mathbf{H}^*_{kf}$ are the numerical fluxes in that face [40]. The DG method can be formulated with different types of numerical fluxes, the centered and upwind fluxes, which are the most commonly used ones [41], [42]. The dispersive and dissipative properties of the solution will greatly depend on the flux choice, allowing for some tuning capability according to the application.

III. CGTD Versus DGTD: The CDGTD Method

From the computational point of view, the main disadvantage of CGTD is that it requires a global linear solver, containing all of the degrees of freedom, to be solved on each time-step. DGTD, in turn, when used in conjunction with an explicit time integration technique, allows for each element to be solved independently, thus drastically reducing the computational burden with respect to CG, making it comparable even to that of classical FDTD [43], [44].

However, there are pros and cons of both methods that make sense trying to build hybrid approaches by taking the best of each one, and they are given as follows.

- A well-known drawback of nodal FEM is the presence of spurious modes [1]. These are commonly attributed to a variety of reasons, including an inexact representation of the underlying de Rham complex [45]–[49]. One way of removing this source of spurious modes is to resort to vector-based formulations [2], [7], [50]. Comparing vector and nodal FEM is beyond the scope of this work; advantages and disadvantages of both of them have been reported in literature [4], [51] and deserve a full work to be further analyzed. Another approach to mitigate spurious modes is by introducing penalty terms associated with the divergence of $\mathbf{E}$ or $\mathbf{H}$ [3], [41], [52], [53], at the cost of adding extra terms, and DOFs, that are to be evolved at each time step [41].
  Spurious nodes are present both in nodal DGTD and CGTD. However, for DGTD, they can be easily mitigated, with a slight increase in computational cost, by using upwind or penalized fluxes instead of centered fluxes, at the cost of introducing some dissipation. This dissipation especially affects spurious modes which are much further attenuated than physical ones [54], thus resulting in a cleaner spectrum and better convergence properties [12], [16], [55]. Centered flux can also be proven to be spurious-free in highly regular meshes [41], though this is not a realistic situation found in a general problem.
- CG nodal methods can drive to globally wrong solutions when singularities or nonconvex domains are present [3], [4]. This has not been observed for DG nodal formulations [41].
- Regarding dissipation, if a symplectic time integrator is used for (2), CG methods are not dissipative, while DG becomes dissipative when combined to upwind/penalized fluxes to remove spurious solutions, as mentioned above.
- CG presents more relaxed stability constraints in the time-step than DG, thanks to the fact that the spectral radius of the assembled system (CG) is smaller than that of the unassembled one (DG) [29]. This is a consequence of the better representation of long-range interactions [56].
- Regarding the number of DOFs, CG presents advantages due to the fact that the nodes on the interface between two elements do not need to be duplicated, as in DG, since CG collapses them to enforce continuity. Furthermore, DG also needs to compute one matrix-vector product for each face of the element at each iteration.
- Finally, the continuous nature of CGTD also makes necessary a special treatment in regions where the electromagnetic properties of the media exhibit abrupt changes [8], while DGTD naturally implements these conditions thanks to the use of fluxes [57], [58].

The discussion above begs the question as to whether one could formulate a hybrid CDG technique that exploits the advantages of both formulations. In [38] a hybrid method is formulated in 2-D. For it, the CG formalism is applied in a large structured region formed of squares, coupled to a DG scheme applied to another region consisting on an unstructured mesh of triangles. The use of a continuous formalism in the large region thus requires the solution of a large global system of equations that reduces the performance of such an approach, especially for large problems.

In contrast, we propose here a new method based on a CG formulation only on multiple, small clusters of elements. As usual in CG, the elements within the cluster remove duplicate DOFs on their boundaries, and they exchange information with adjacent clusters, or single elements, through classical numerical fluxes in a DG manner. As a result, CG clusters are decoupled among them, and the whole domain can be solved by an explicit marching-on-in-time algorithm. In this work, we will analyze the tradeoffs of using these CG clusters, which have to be sufficiently small both to keep the system of equations frontally invertible and to avoid spurious modes, and as large as possible to reduce the DOFs, enhance the dissipation, and increase the time-step for stability. If upwind numerical fluxes are employed for the DG connection, the CDG method is expected to be spurious-free, partially inheriting from CG the aforementioned advantages.

In the remainder of this paper, we will assume a translational symmetry by meshing regions with clusters that are identical to each other. Though this is not strictly necessary, in general, it is actually a desirable property, since it allows us to compute the semi-discretized operators for a single cluster and reuse it for the rest thus saving memory. Hence, the kind of meshes that would benefit most of this clustering would be structured or semi-structured, as further discussed in the Conclusions. This is also true of multi-element approaches [26]–[28] in which a reduction of DOFs and increased time-step can be likewise achieved [59]. In the rest of the mesh, we apply the usual unstructured DG formalism. We can write the final scheme in matrix notation as

$$\begin{aligned} \mathcal{M}_c \partial_t \mathbf{E}_c(t) + \mathcal{S}_c \mathbf{H}_c(t) - \sum_f^{N_{fc}} \mathcal{F}_{cf} \mathbf{H}^*_{cf}(t) = 0 \\ \mathcal{M}_c \partial_t \mathbf{H}_c(t) - \mathcal{S}_c \mathbf{E}_c(t) + \sum_f^{N_{fc}} \mathcal{F}_{cf} \mathbf{E}^*_{cf}(t) = 0 \end{aligned} \tag{4}$$

where $\mathcal{M}_c = \mathcal{Z}_c \mathcal{M}_{k_c} \mathcal{Z}_c^T$ and $\mathcal{S}_c = \mathcal{Z}_c \mathcal{S}_{k_c} \mathcal{Z}_c^T$ are the mass and stiffness operators assembled as in the CG method but using only the elements k_c belonging to the cluster c. The operators $\mathcal{F}_{cf}$ are constructed in the same way as for the DG method but considering only the N_{fc} external faces of the cluster.

IV. Numerical Properties

In order to perform a semi-analytical study of CDGTD, we will follow a similar approach to [9], [29], [42] for analyzing the dispersive properties of our method in 1-D. To do so, we seek spatially periodic solutions of the form

$$\begin{aligned} E(t,x) = E_0 e^{(i(lx-\omega t)} \\ H(t,x) = H_0 e^{(i(lx-\omega t)} \end{aligned} \tag{5}$$

that are supported by the spatial semi-discretization. The computational domain Ω is split into K_c elements of equal length h. These K_c elements are assembled in the same way as indicated by (4). We also define a state vector $\mathbf{q}_c = [\mathbf{E}_c, \mathbf{H}_c]^T$ containing

all of the N_c DOFs in a cluster c. The elements at the end positions of the computational domain are connected assuming periodic solutions of the form

$$\begin{aligned}\mathbf{e}_0^T\mathbf{q}_{c+1} &= e^{ilhK_c}\mathbf{e}_{N_c}^T\mathbf{q}_c\\ \mathbf{e}_{N_c}^T\mathbf{q}_{c-1} &= e^{-ilhK_c}\mathbf{e}_0^T\mathbf{q}_c\end{aligned} \tag{6}$$

and using the DG numerical flux formalism to treat the boundaries of the cluster as if they were neighboring other clusters. We will use the factor $L = lh$ as the normalized numerical wavenumber. With these assumptions, we can reformulate (4) as

$$\partial_t\mathbf{q}_c(t) = (\mathcal{M}_c^q)^{-1}\left(\mathcal{S}_c^q - \sum_f \mathcal{F}_{cf}^q\mathcal{E}_{cf}(L)\right)\mathbf{q}_c(t). \tag{7}$$

A diagonal operator $\mathcal{W}$ containing the spectrum of eigenfrequencies is obtained by a similarity transformation via an invertible operator $\mathcal{P}$ to obtain

$$\mathcal{W} = i\,\mathcal{P}^{-1}\,(\mathcal{M}_c^q)^{-1}\left(\mathcal{S}_c^q - \sum_f \mathcal{F}_f^q\mathcal{E}_{cf}(L)\right)\mathcal{P} \tag{8}$$

We can also define the eigenstates of the system as

$$\mathbf{p}_c = \mathcal{P}^{-1}\mathbf{q}_c. \tag{9}$$

This change of basis lets us write (7) in the following compact form:

$$\partial_t\mathbf{p}_c(t) = -i\,\mathcal{W}(L)\mathbf{p}_c(t) \tag{10}$$

with semi-discrete solutions of the form

$$\mathbf{p}_c(t) = e^{-i\mathcal{W}(L)t}\mathbf{p}_c(0). \tag{11}$$

The $j = 0,\ldots,N_c$ eigenvalues ω_j of $\mathcal{W}$ correspond to the eigenfrequencies of the discrete periodic problem.

The real part $\Re[\omega_j]$ corresponds to the oscillating frequency and the imaginary part $\Im[\omega_j]$ corresponds to the numerical dissipation or amplification of eigenstate j, if any. For all Galerkin methods studied here, we have $\Im[\omega_j] \leq 0$, which is a necessary condition for stability. The phase velocities supported by the scheme are $c_j(L) = \omega_j h/L$. As in our system of units, the speed of light is 1, and we will consider that the mode with phase velocity closest to one is the free-space mode. Therefore, we expect that

$$\lim_{L\to 0} c_{(\mathrm{fs})}(L) = 1. \tag{12}$$

The study of the full spectrum of $\mathcal{W}$ is also useful as its properties impose limitations with regard to the time-integration. The LF2 method [60] has the following stability requirement on its time step h_t:

$$h_t \leq 1/\Re[\omega_j]\;\forall j \tag{13}$$

and therefore will be constrained by the largest real part among all eigenvalues. LSERK methods comprise irregular closed loci in the complex plane [16], [61], in which the eigenvalues must lie to ensure stability. Thus, to warranty stability, the following condition must be enforced for each cluster:

$$\max|\omega_j| \leq \rho(h_t)\;\forall j \tag{14}$$

where ρ is the spectral radius of the LSERK method.

A. Convergence

Figs. 1 and 2 show a comparison of the convergence rates on the dispersion curves for the DG and CDG schemes with clusters of two and three elements and for upwind and centered fluxes, found with the procedure described above. These convergence rates have been calculated for orders ranging from $P = 1$ to 3. Table I summarizes the convergence rates where the component dominating in the global error has been highlighted. In agreement with what is found for P refinements of centered DG schemes [42], the convergence rate of CDG depends on the number of elements assembled with an even–odd pattern. With an odd number of elements, CDG with upwind and centered fluxes have the same convergence rates as classical DG methods. For upwind CDG schemes with an even number of elements, we see an alternating dominance of the error showing that CDG has a better global convergence for odd orders of P. Please note that convergence rates depending on even/odd parameters has been previously in DG analysis [42].

The case of centered CDG with an even number of elements shows that it has the same $2P+3$ convergence as the upwind DG scheme, therefore improving significantly versus its centered DG counterpart. Note that for upwind fluxes, spurious modes are also rapidly attenuated in CDG and therefore should not impact the time-domain solution, similarly as observed in [9], [54] for the DG case [cf. Fig. 5, which shows that the free-space mode observed is much less attenuated than any other supported mode].

B. Spectral Properties

Fig. 3 shows the full spectrum of DG and CDG operators with two and three elements and upwind fluxes. Fig. 4 shows the effect in the spectrum of increasing the number of elements. The maximum real part, and the spectral radii of the different schemes are presented in Table II. We note that the CDG assembling, even for a moderate number of elements, reduces significantly the spectral radius to approximately one half of that of the DG. As mentioned above, this allows for a larger time step to be used.

V. Computational Cost

This section presents some estimates about the number of DOF and computational operations needed for several configurations (Fig. 6) in which we can apply the aforementioned translational symmetry.

The number of clustered elements and their order have a critical impact on the number of operations required to evaluate the semi-discretized operators in CDG. For this reason, only relatively small clusters with low orders are studied. Moreover, the greater the number of inner faces the cluster has, the greater the number of DOFs and numerical fluxes eliminated. Fig. 6 shows the 2-D and 3-D clusters studied in this work that exemplify such properties.

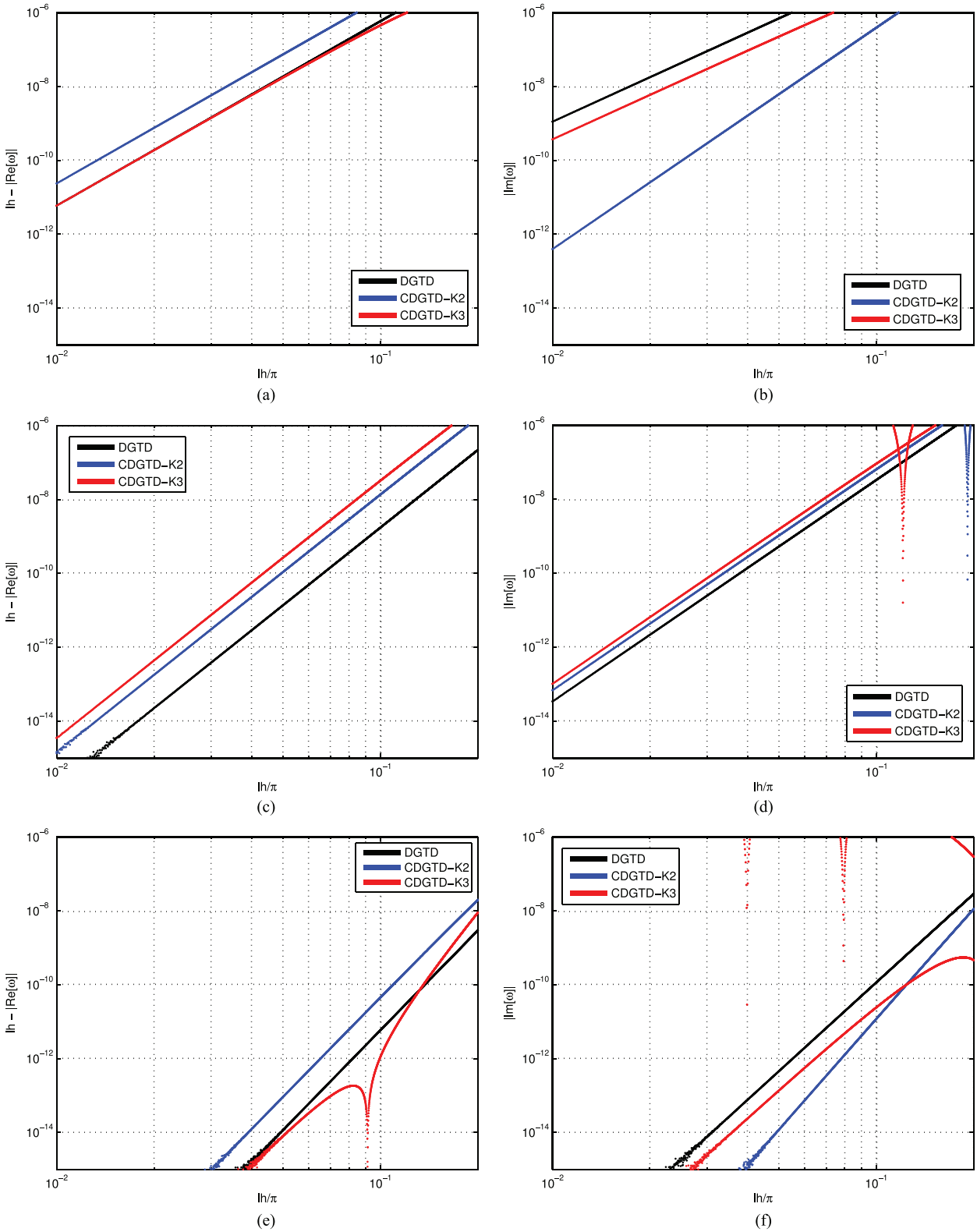

Fig. 1. Convergence rates for DGTD and CDGTD schemes with upwind fluxes. Dispersion and dissipation errors are represented in the first and second columns, respectively. Nonaligned values correspond to other modes also supported by the solutions but that do not correspond to the free-space mode. (a) Dispersion for $P = 1$. (b) Dissipation for $P = 1$. (c) Dispersion for $P = 2$. (d) Dissipation for $P = 2$. (e) Dispersion for $P = 3$. (f) Dissipation for $P = 3$.

Tables III and IV show a comparison of the CDG and DG methods for different kinds of elements and cluster configurations. We observe that the clustering always causes a reduction in the DOF by eliminating the need of having duplicated nodes at the interfaces within the cluster. In 3-D, the reduction is more significant, e.g., for the cross-hatch cluster with $P = 1$ we have a reduction of about 80%. The number of operations for the lift operations scale as $KN_fN_pN_{fp}$ and for the

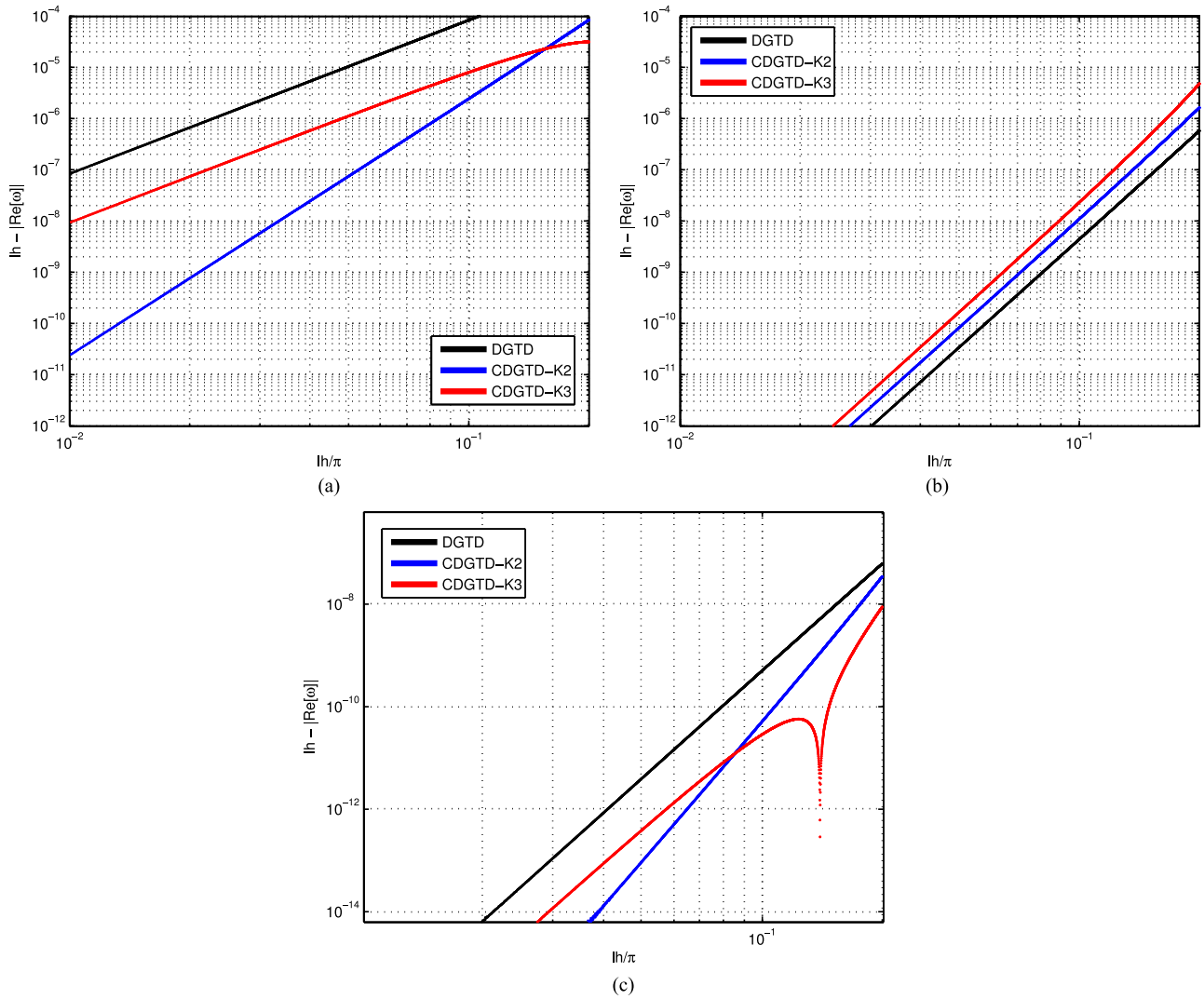

Fig. 2. Convergence rates for dispersion errors of DGTD and CDGTD schemes with centered fluxes. (a) $P = 1$. (b) $P = 2$. (c) $P = 3$.

TABLE I
CONVERGENCE RATES USING UPWIND AND CENTERED FLUXES. HIGHLIGHTED CELLS INDICATE THE DOMINANT TERM

		DGTD		CDGTD K_c even		CDGTD K_c odd	
	P	$\Re[\tilde{\omega}]$	$\Im[\tilde{\omega}]$	$\Re[\tilde{\omega}]$	$\Im[\tilde{\omega}]$	$\Re[\tilde{\omega}]$	$\Im[\tilde{\omega}]$
Upwind	1	5	4	5	6	5	4
	2	7	6	7	6	7	6
	3	9	8	9	10	9	8
	4	11	10	11	10	11	10
Centered	1	3	–	5	–	3	–
	2	7	–	7	–	7	–
	3	7	–	9	–	7	–
	4	11	–	11	–	11	–

curl operations as $2KN_p^2$. The cost of computing the numerical fluxes $\mathbf{E}^*$ and $\mathbf{H}^*$ has not been included as it encompasses only vector-vector operations. For $P \leq 2$ the estimates show that the number of operations needed per time step is similar for both methods. For higher orders, the term N_p starts to dominate and the CDGTD method becomes less attractive compared with the classical DGTD approach. However, it should be noted that CDG operators have a reduced spectral radius that allows for a larger time step, as will be shown in Section VI. Moreover, in many cases the bottleneck in speed is related to the memory bandwidth and data locality. Therefore, having a reduced number of DOF that are also contiguous in memory may result in additional speed-up, as discussed in [21]. The use of the same spatial operators also alleviates the memory bandwidth, additionally ideally they can remain in the CPU cache during the evaluation of the whole clusters. Finally, the fact that the operator spectrum has a smaller imaginary part when upwind fluxes are used suggests that the scheme can further benefit from the use of different LSERK schemes [16] that allow for a larger time step.

Another question that may arise regarding computational efficiency is how the configurations under study compare with the use of a single element covering the same space, i.e., quadrilaterals (quads) in 2-D or hexahedrons (hex) in 3-D. Tables III and IV show a comparison of the estimated numbers of operations for different orders and dimensions. As it may be appreciated, for the 3D case, the simple-hatch configuration has the same number of DOFs and needs the same amount of operations to calculate the curl than a hex cell of the same order. There is

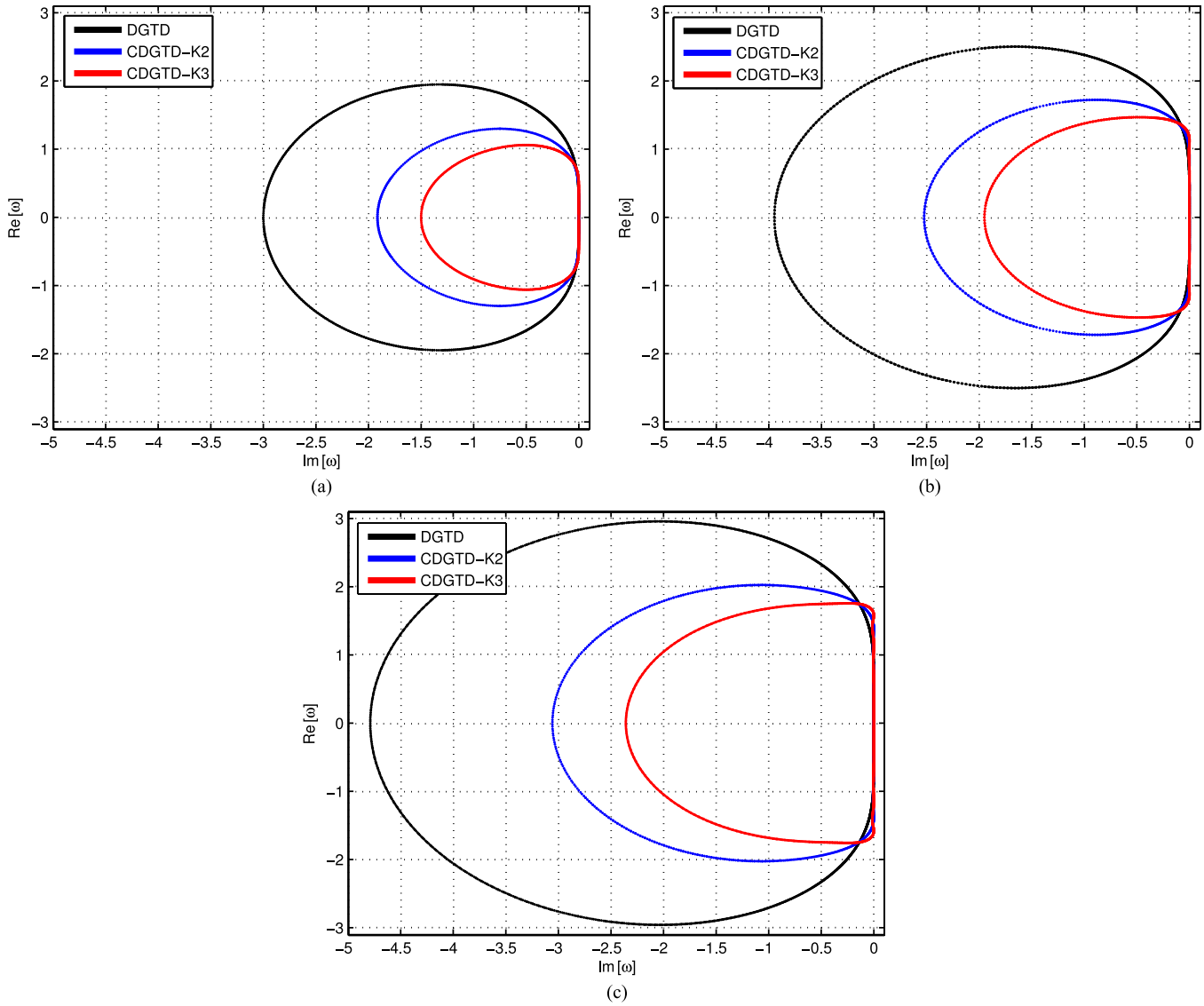

Fig. 3. Eigenvalues spectrum loci for upwind fluxes schemes with polynomial basis up to order $P = 3$. (a) $P = 1$. (b) $P = 2$. (c) $P = 3$.

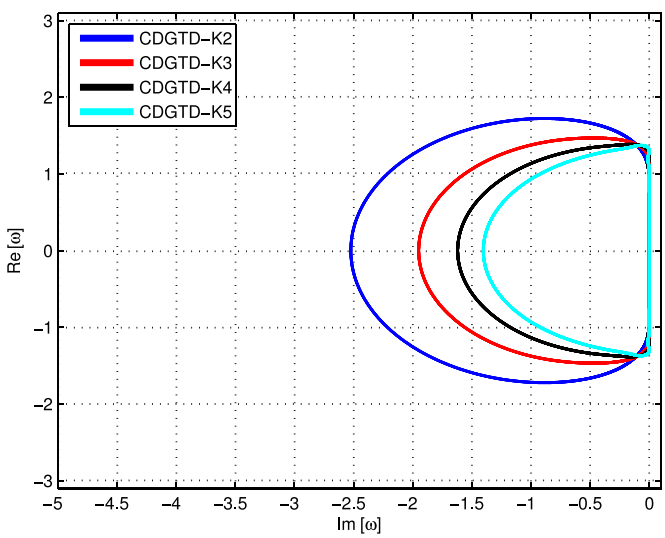

Fig. 4. Eigenvalues spectrum loci for upwind fluxes schemes with polynomial basis of order $P = 2$, for different numbers of elements clustered.

an increase in the number of operations needed to calculate the LIFT because the increased number of faces, but this is partially compensated with a reduced N_{fp}. The cross-hatch clusters have a similar number of DOFs and need a similar number of operations than a hex cell of one order higher.

VI. Numerical Test: 2-D Cavity

A. Resonances

Fig. 7 shows the results of simulating a unit square cavity using CGTD, DGTD, and CDGTD using a cross-hatch clustering. The simulation runs up to a final time $T = 200$, with a basis order of $P = 2$ and a cross-hatch grid mesh with $h = 1/8$. The time integration was performed with the same LSERK4 scheme used in the previous section. The cavity was excited with a white noise similarly as in [11], [15]. As discussed in the Introduction, CGTD presents spurious modes that pollute the spectrum, with the most important being visible at $\omega \simeq 2$ and 2.2. When centered fluxes are used, CDGTD also exhibits some

TABLE II
MAXIMUM REAL PARTS AND SPECTRAL RADIUS. THE INCREASE ON CLUSTERED ELEMENTS ALLOWS THE USE OF LARGER TIME STEPS. NOTE THAT, FOR CENTERED FLUXES, THE IMAGINARY PART IS ALWAYS ZERO UP TO MACHINE PRECISION AND THEREFORE THE SPECTRAL RADIUS IS EQUAL TO THE MAXIMUM REAL VALUE

		DGTD		CDGTD $K_c = 2$		CDGTD $K_c = 3$		CDGTD $K_c = 4$	
	P	$\max \lvert\Re[\tilde{\omega}]\rvert$	$\rho[\tilde{\omega}]$	$\max \lvert\Re[\tilde{\omega}]\rvert$	$\rho[\tilde{\omega}]$	$\max \lvert\Re[\tilde{\omega}]\rvert$	$\rho[\tilde{\omega}]$	$\max \lvert\Re[\tilde{\omega}]\rvert$	$\rho[\tilde{\omega}]$
Upwind	1	1.95	3.00	1.30	1.92	1.06	1.50	0.94	1.25
	2	2.50	3.95	1.72	2.52	1.47	1.95	1.39	1.62
	3	2.96	4.79	2.03	3.06	1.76	2.36	1.74	1.96
	4	3.37	5.57	2.29	3.54	2.03	2.73	2.05	2.27
Centered	1	2.00		1.50		1.35		1.29	
	2	2.69		2.18		1.06		2.02	
	3	3.32		2.79		2.68		2.66	
	4	3.94		3.38		3.30		3.28	

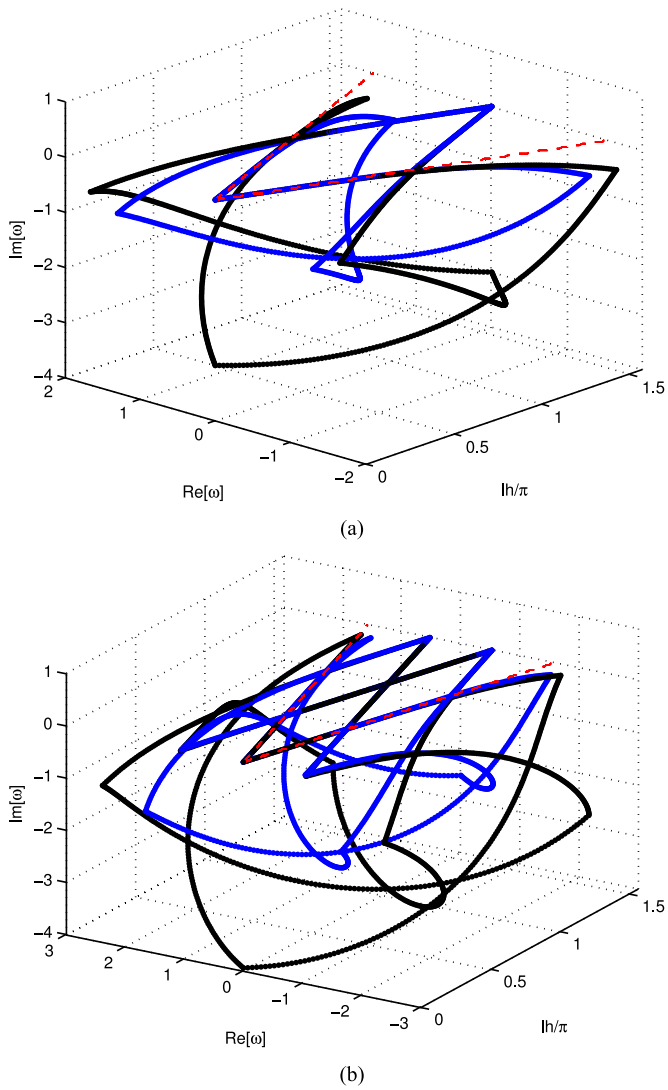

Fig. 5. Eigenvalues spectrum loci for upwind fluxes schemes with polynomial basis of different order for DGTD (black) and CDGTD with $K_c = 2$ (blue) schemes. As it can be seen, modes that do not belong to the physical eigenspectrum (dashed lines) have large imaginary parts and are therefore quickly attenuated. (a) $P = 1$. (b) $P = 2$.

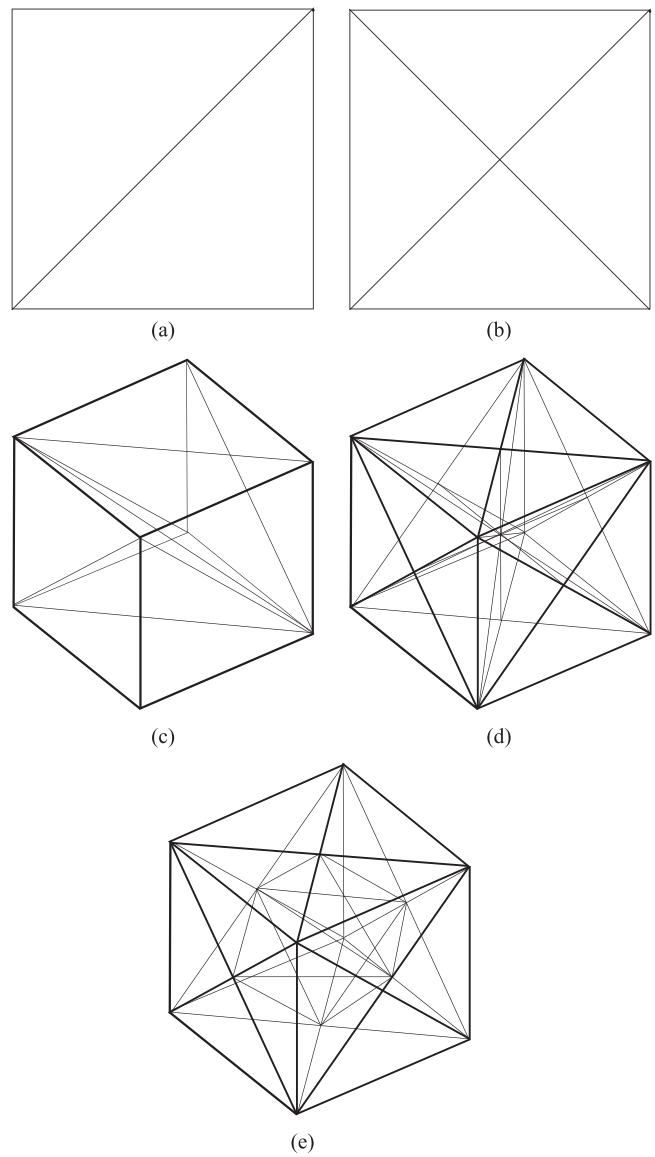

Fig. 6. Different clusters assemblies considered for 2-D and 3-D CDG. (a) Simple-hatch. (b) Cross-hatch. (c) Simple-hatch in 3-D, 6 tetrahedrons. (d) Cross-hatch in 3-D, 24 tetrahedrons. (e) Anisotropic Cross-hatch in 3-D, 24 tetrahedrons.

pollution of the spectrum. A small spurious mode appears at $\omega \simeq 1.7$, and a larger one appears in $\omega \simeq 3.3$. The use of upwind fluxes eliminates this problem at all frequencies considered, as expected from our previous discussion.

TABLE III
DOF AND A ESTIMATION OF THE COMPUTATIONAL COSTS OF THE DGTD AND CDGTD SCHEMES FOR A 2-D CROSS-HATCH CLUSTER

	Quad cell			Cross-hatch						Simple-hatch			
	DGTD2D			DGTD2D			CDGTD2D			DGTD2D		CDGTD2D	
P	1	2	3	1	2	3	1	2	3	1	2	1	2
DOF	4	9	16	12	24	40	5	13	25	6	12	4	9
LIFT	32	108	256	72	216	480	24	156	400	36	108	32	108
Curl	32	162	512	72	288	800	50	338	1250	36	144	32	162
Total	64	270	768	144	504	1280	64	494	1650	72	262	64	270

TABLE IV
DOF AND A ESTIMATION OF THE COMPUTATIONAL COSTS OF THE DGTD AND CDGTD SCHEMES FOR A 3-D CROSS-HATCH CLUSTER

	Hex cell			Cross-hatch				Anisotropic cross-hatch		Simple-hatch			
	DGTD3D			DGTD3D		CDGTD3D		CDGTD3D		DGTD3D		CDGTD3D	
P	1	2	3	1	2	1	2	1	2	1	2	1	2
DOF	8	27	64	96	240	15	65	14	63	24	60	8	27
LIFT	192	1458	6144	1152	5760	1080	9360	1008	4536	288	1440	288	1944
Curl	128	1458	8192	768	4800	450	8450	392	7938	192	1200	128	1458
Total	320	2916	14336	1920	10560	1530	17810	1400	12474	480	2640	416	3402

B. Convergence With Respect to h-Refinement

Table V shows the results of calculating the L^2 error norm in a square cavity using

$$\|E - E_h\|_{\Omega_h} = \left(\sum_k \int_{\Omega_k} \|E_e - E_h\|^2 d\Omega_k \right)^{\frac{1}{2}} \tag{15}$$

where E_e is the exact (analytical) solution, and E_h is the numerical solution. The L^2 error norm is calculated after exciting the first mode of the cavity as initial condition in square meshes of sizes $[0,1] \times [0,1]$ with different cell sizes and evolving the scheme up to a final time $T = 4/\sqrt{2}$ (two cycles). Two of the meshes used for these computations are shown in Fig. 8, where the pattern followed for the refinement can be inferred from. The computations have been carried out with upwind and centered fluxes using spatial basis with P from 1 to 3. For CDGTD the clustering has been done using the cross-hatch configuration. For upwind and centered fluxes, we see a clear improvement for $P = 1$ in the convergence rate of the L^2 error norm as it improves from $\sim$2.4 to $\sim$3.2. For higher orders the results present a similar convergence rate with the exception of $P = 2$ for centered flux in which CDG produce a considerably higher error. The time integration was done using an LSERK4 scheme where h_t has been set heuristically and we find that for upwind fluxes the h_t for CDGTD can be set $\sim$50% larger than for DGTD. With centered fluxes the gain is more moderate ($\sim$20%). As expected, CDGTD used much less DOF, varying from $\sim$40 to $\sim$60% less depending on P.

Note that, although some improvements are achieved with CDGTD, if we compare results between different orders the DGTD method shows that better results can be achieved with DGTD for a similar number of DOFs by increasing the basis order. For example, if we compare the upwind cases of DGTD with $P = 3$ and $h = 1/8$ and CDGTD with $P = 2$ and $h = 1/16$, we observe that DGTD achieves a smaller error than CDGTD using less DOFs. However, CDGTD allows a larger h_t for stability, and needs less number of operations, according to Table III.

VII. APPLICABILITY SCENARIOS

From the analysis performed in this paper, some applicability scenarios can be devised where the use of CDGTD in certain parts of the mesh may be of interest.

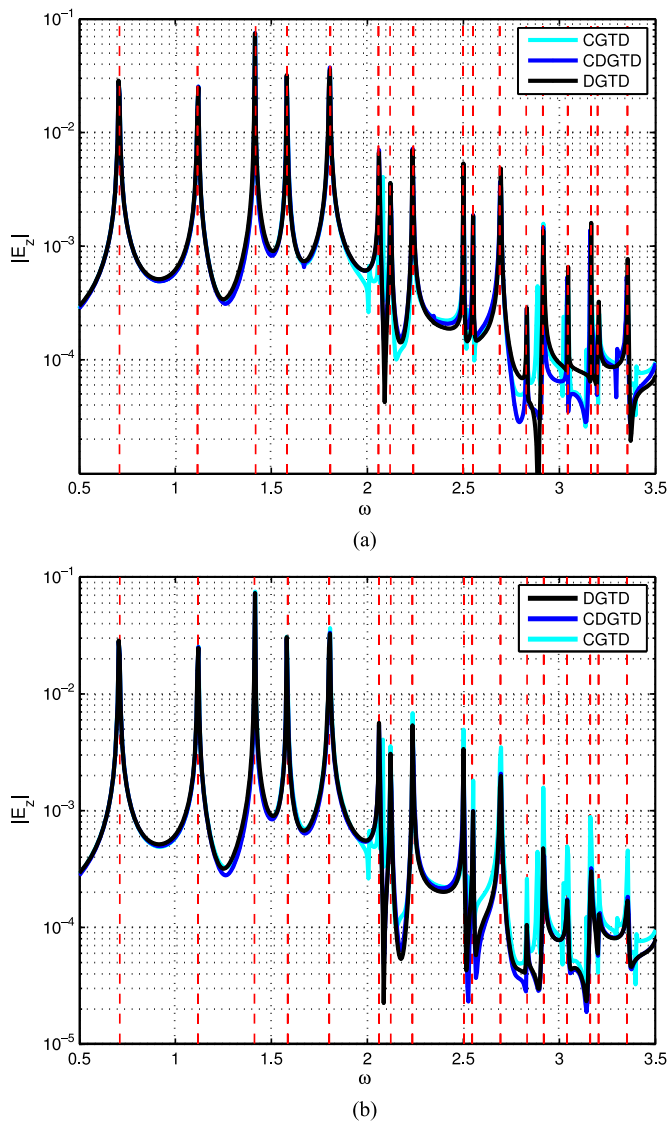

Fig. 7. Resonances in a unit square PEC cavity for different methods. The simulations run up to a final time $T = 200$. The basis order is $P = 2$ and the mesh is a cross-hatch grid with $h = 1/8$. The CDGTD results have been obtained by clustering all cross-hatch cells. With centered fluxes, the CGTD and CDGTD method have some visible spurious modes polluting the spectrum at $\omega \simeq 1.7, 2.2, 2.8 \ldots$. (a) Centered flux. (b) Upwind flux.

TABLE V
L^2 ERROR NORM FOR DIFFERENT RESOLUTIONS OF THE FIRST MODE OF A UNIT SQUARE CAVITY AFTER A SIMULATED TIME OF $4/\sqrt{2}$ (TWO CYCLES). FOR ALL CDGTD CASES, THE TIME STEPS CAN BE LARGER THAN THOSE FOR DGTD, WITH SMALLER IMPROVEMENTS FOR CENTERED THAN FOR UPWIND FLUX. THE NUMBER OF DOFS WITH THE CDGTD CROSS-HATCH CONFIGURATION ARE 40%∼60% LESS DEPENDING ON THE SPATIAL ORDER. CONVERGENCE RATIOS REMAIN SIMILAR FOR ALL CASES, EXCEPT FOR THE CASE $P = 1$, WHERE A CLEAR IMPROVEMENT IS OBSERVED

	P	h	DGTD				CDGTD Cross-hatch			
			L^2 Error	Order	h_t	DOF	L^2 Error	Order	h_t	DOF
Upwind	1	1/2	4.6E-2	-	120E-3	48	3.7E-2	-	197E-3	20
		1/4	1.2E-3	2.5	60E-3	192	1.5E-4	3.8	98E-3	80
		1/8	3.0E-5	2.6	30E-3	768	1.2E-6	3.3	49E-3	320
		1/16	1.1E-6	2.3	15E-3	3072	1.7E-8	3.0	25E-3	3072
		1/32	5.9E-8	2.0	7E-3	12288	2.6E-10	2.9	12E-3	5120
	2	1/2	1.2E-4	-	595E-4	96	1.7E-4	-	984E-4	52
		1/4	1.5E-6	3.0	298E-4	384	1.9E-6	3.1	492E-4	208
		1/8	2.3E-8	2.9	149E-4	1536	2.3E-8	3.1	246E-4	832
		1/16	3.6E-10	2.9	74E-4	6144	3.4E-10	2.9	123E-4	3328
		1/32	5.6E-12	2.9	37E-4	24576	5.2E-12	2.9	61E-4	13312
	3	1/2	1.2E-6	-	397E-4	160	2.8E-6	-	656E-4	100
		1/4	5.2E-9	3.8	198E-4	640	7.5E-9	4.1	328E-4	400
		1/8	2.1E-11	3.8	99E-4	2560	2.0E-11	4.1	164E-4	1600
		1/16	8.2E-14	3.8	50E-4	6400	8.6E-14	3.8	82E-4	6400
		1/32	3.2E-16	3.8	25E-4	40960	2.8E-16	4.0	41E-4	25600
Centered	1	1/2	2.4E-2	-	166E-3	48	4.3E-3	-	197E-3	20
		1/4	9.6E-4	2.2	83E-3	192	9.4E-4	1.1	98E-3	80
		1/8	5.6E-5	2.0	41E-3	768	1.5E-6	4.5	49E-3	320
		1/16	3.5E-6	1.9	21E-3	3072	1.7E-8	3.1	25E-3	3072
		1/32	2.2E-7	1.9	10E-3	12288	2.6E-10	2.9	12E-3	5120
	2	1/2	1.7E-4	-	776E-4	96	1.2E-4	-	984E-4	52
		1/4	2.8E-6	2.8	388E-4	384	4.6E-5	0.7	492E-4	208
		1/8	4.2E-8	2.9	194E-4	1536	2.3E-6	2.1	246E-4	832
		1/16	6.6E-10	2.9	97E-4	6144	9.4E-8	2.2	123E-4	3328
		1/32	1.0E-11	2.9	49E-4	24576	5.2E-9	2.0	61E-4	13312
	3	1/2	1.8E-6	-	518E-4	160	7.9E-6	-	656E-4	100
		1/4	7.1E-9	3.8	259E-4	640	5.3E-9	5.1	328E-4	400
		1/8	2.1E-11	4.0	129E-4	2560	1.3E-10	2.6	164E-4	1600
		1/16	1.2E-13	3.6	65E-4	6400	4.0E-13	4.0	82E-4	6400
		1/32	3.4E-16	4.1	32E-4	40960	1.4E-15	3.9	41E-4	25600

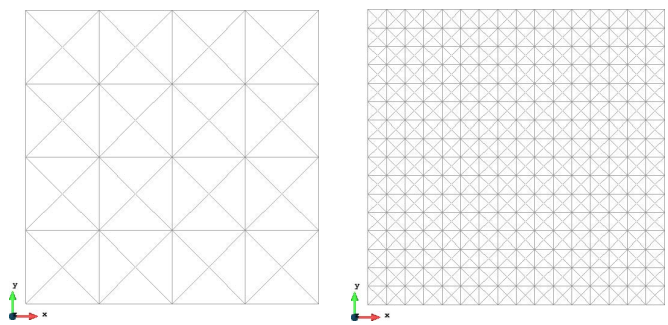

(a) (b)

Fig. 8. $h = 1/4$ and $h = 1/16$ meshes used to compute the resonant cavity results. Each of the cross-hatch elements is assembled to form a cluster. (a) $h = 1/4$. (b) $h = 1/16$.

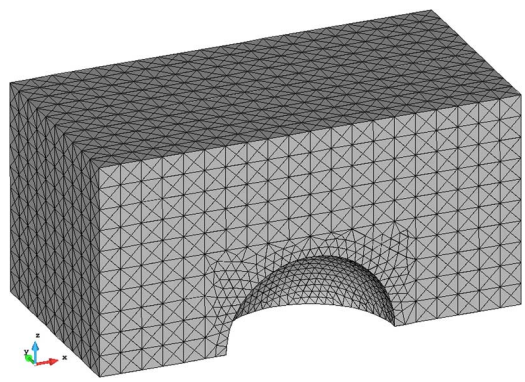

Fig. 9. Suitable partially structured mesh in which the CDGTD formalism would preferably be used only in cross-hatch regular tetrahedron clusters.

1) **DOF reduction in structured regions**: The discussion carried out in Section V shows that using semi-structured arrangements of CDG clusters can drastically reduce the number of DOFs for any P. Fig. 9 shows a situation in which the use of the CDGTD method could improve performance. When used in this way, an added advantage of the CDGTD formulation with respect to multi-element meshes is that the clusters can exist in many different configurations, it suffices for them to have translational symmetry to fully cover a region of the space. If we compare with the costs associated to hex cells we see that we can have benefits similar to the use of hybrid meshes using exclusively tetrahedral meshes while we retain their geometric flexibility. Note also that obtaining and operating with a mesh formed exclusively of tetrahedrons is significantly simpler than with hybrid meshes.
2) **Buffering between element types**: Multi-element approaches exploit the advantages of, mainly, tetrahedral and hexahedral mesh elements. In three-dimensional problems this forces the use of nonconforming interfaces [26], [27] or the use of pyramidal elements [28] for the transitions between elements of different types. CDGTD can offer a solution to do these transitions by using a simple-hatch cluster [Fig. 6(c)] between tetrahedral and

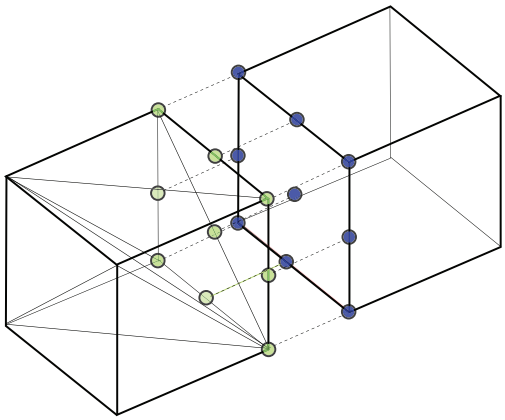

Fig. 10. Interfacing between the simple-hatch cluster and a hex cell for $P = 2$.

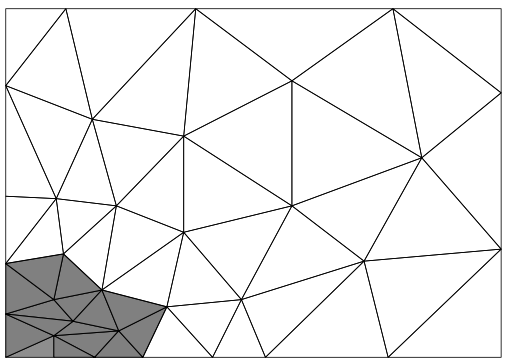

Fig. 11. Region with high stiffness (grayed) can be assembled into a CDG cluster to improve the maximum time step allowed. The rest of the mesh can be evolved using a classical DGTD scheme.

hexahedral regions (Fig. 10). When using nodal functions, the interfacing is simplified because rather than having multivalued nodes at the diagonal of the tetrahedral region, we have a single one. This avoids the need of performing an interpolation or use a nonconformal boundary. We can directly use the DOFs belonging to the nodes in contact in order to compute the fluxes.

3) **Reduction of high stiffness time constraints**: CDGTD formalism can also be used to assemble stiff elements to alleviate their time step constraints. As shown in Section VI the assembling produces a significant reduction of the size of the spectrum letting us to increase the time step used. This can drive to a significant gain in certain situations (Fig. 11) because the maximum time step is constrained by the maximum allowed time step of the smallest element.

VIII. Conclusion

In this work, we have introduced a new hybrid CDG method for Maxwell's curl equations and studied some of its numerical properties. The CDG method facilitates the use of implicit techniques in TD, requires less DOF than conventional DG and allows for larger time-steps. The overall number of operations needed is also reduced for certain configurations and for low orders. Combined with improvements in memory locality leaves open the possibility that the method is computationally more affordable than pure DG, at least up to order $P = 2$. Some applicability scenarios for this technique have been proposed.

References

[1] P. P. Silvester and R. L. Ferrari, *Finite Elements for Electrical Engineers*, 3rd ed. Cambridge, U.K.: Cambridge Univ., 1996.

[2] J. Jin, *The Finite Element Method in Electromagnetics*. New York, NY, USA: Wiley-Interscience, 1993.

[3] M. Costabel and M. Dauge, "Weighted regularization of Maxwell equations in polyhedral domains," *Numerische Mathematik*, vol. 93, pp. 239–277, 2002.

[4] R. Otin, "Regularized Maxwell equations and nodal finite elements for electromagnetic field computations," *Electromagn.*, vol. 30, pp. 190–204, 2010.

[5] J. Nedelec, "Mixed finite elements in R3," *Numerische Mathematik*, vol. 35, no. 3, pp. 315–341, 1980.

[6] J. Nedelec, "A new family of mixed finite elements in R3," *Numerische Mathematik*, vol. 50, no. 1, pp. 57–81, 1986.

[7] D. Sun, J. Manges, X. Yuan, and Z. Cendes, "Spurious modes in finite-element methods," *IEEE Antennas Propag. Mag.*, vol. 37, pp. 12–24, Oct. 1995.

[8] J.-F. Lee, R. Lee, and A. Cangellaris, "Time-domain finite-element methods," *IEEE Trans. Antennas Propag.*, vol. 45, no. 3, pp. 430–442, Mar. 1997.

[9] J. S. Hesthaven and T. Warburton, *Nodal Discontinuous Galerkin Methods: Algorithms, Analysis, Applications*, 1st ed. New York, NY, USA: Springer, 2007.

[10] S. Gedney, T. Kramer, C. Luo, J. Roden, R. Crawford, B. Guernsey, J. Beggs, and J. Miller, "The discontinuous Galerkin finite element time domain method (DGFETD)," in *Proc. IEEE Int. Symp. Electromagn. Compatibility*, Aug. 2008, pp. 1–4.

[11] J. Kim and F. Teixeira, "Parallel and explicit finite-element time-domain method for Maxwell's equations," *IEEE Trans. Antennas Propag.*, vol. 59, no. 6, pp. 2350–2356, Jun. .

[12] E. Montseny, S. Pernet, X. Ferriéres, and G. Cohen, "Dissipative terms and local time-stepping improvements in a spatial high order discontinuous Galerkin scheme for the time-domain Maxwell's equations," *J. Computational Phys.*, vol. 227, pp. 6795–6820, Jul. 2008.

[13] S. Piperno, "Symplectic local time-stepping in non-dissipative DGTD methods applied to wave propagation problems," *ESAIM: Math. Modelling Numer. Anal.*, vol. 40, pp. 815–841, 2007, 1.

[14] S. Dosopoulos, "Interior penalty discontinuous Galerkin finite element method for the time-domain Maxwell's equations," Ph.D. dissertation, Dept. Electr. Comput. Eng., Ohio State Univ., Columbus, OH, USA, 2012.

[15] L. D. Angulo, J. Alvarez, F. Teixeira, M. Pantoja, and S. Garcia, "Causal-path local time-stepping in the discontinuous Galerkin method for Maxwell's equations," *J. Computational Phys.*, vol. 256, pp. 678–695, 2014.

[16] R. Diehl, K. Busch, and J. Niegemann, "Comparison of low-storage Runge-Kutta schemes for discontinuous Galerkin time-domain simulations of Maxwell's equations," *J. Computational Theoretical Nanosci.*, vol. 7, no. 8, pp. 1572–1580, 2010.

[17] K. Busch, M. Konig, and J. Niegemann, "Discontinuous Galerkin methods in nanophotonics," *Laser & Photon. Rev.*, vol. 5, no. 6, pp. 773–809, 2011.

[18] B. Cockburn, F. Li, and C.-W. Shu, "Locally divergence-free discontinuous Galerkin methods for the Maxwell equations," *J. Computational Phys.*, vol. 194, pp. 588–610, Mar. 2004.

[19] J. Niegemann, W. Pernice, and K. Busch, "Simulation of optical resonators using DGTD and FDTD," *J. Opt. A: Pure Appl. Opt.*, vol. 11, no. 11, p. 114015, 2009.

[20] H. Fahs, A. Hadjem, S. Lanteri, J. Wiart, and M.-F. Wong, "Calculation of the SAR induced in head tissues using a high-order DGTD method and triangulated geometrical models," *IEEE Trans. Antennas Propag.*, vol. 59, no. 8, pp. 4669–4678, Aug. 2011.

[21] A. Klockner, T. Warburton, and J. Hesthaven, "High-order discontinuous Galerkin methods by GPU metaprogramming," in *GPU Solutions to Multi-scale Problems in Science and Engineering*, ser. Lecture Notes in Earth Syst. Sci., D. A. Yuen, L. Wang, X. Chi, L. Johnsson, W. Ge, and Y. Shi, Eds. Berlin, Germany: Springer, 2013, pp. 353–374.

[22] V. Dolean, H. Fahs, L. Fezoui, and S. Lanteri, "Locally implicit discontinuous Galerkin method for time domain electromagnetics," *J. Computational Phys.*, vol. 229, pp. 512–526, Jan. 2010.

[23] A. Kanevsky, M. H. Carpenter, D. Gottlieb, and J. S. Hesthaven, "Application of implicit-explicit high order Runge–Kutta methods to discontinuous-Galerkin schemes," *J. Computational Phys.*, vol. 225, no. 2, pp. 1753–1781, 2007.
[24] D. Kosloff and H. Tal-Ezer, "A modified Chebyshev pseudospectral method with an O(N-1) time step restriction," *J. Computational Phys.*, vol. 104, no. 2, pp. 457–469, 1993.
[25] T. Warburton and T. Hagstrom, "Taming the CFL number for discontinuous Galerkin methods on structured meshes," *SIAM J. Numer. Anal.*, vol. 46, no. 6, pp. 3151–3180, 2008.
[26] C. Durochat, S. Lanteri, and C. Scheid, "High order non-conforming multi-element discontinuous Galerkin method for time domain electromagnetics," *Appl. Math. Computation*, vol. 224, pp. 681–704, Nov. 2013.
[27] R. Leger, J. Viquerat, C. Durochat, C. Scheid, and S. Lanteri, "A parallel non-confoming multi-element DGTD method for the simulation of electromagnetic wave interaction with metallic nanoparticles," *J. Computational Appl. Math.*, no. 0, 2013.
[28] M. Bergot and M. Duruflé, "Higher-order discontinuous Galerkin method for pyramidal elements using orthogonal bases," *Numer. Methods for Partial Differential Equations*, vol. 29, no. 1, pp. 144–169, 2013.
[29] S. Sherwin, "Dispersion analysis of the continuous and discontinuous Galerkin formulations.," in *Proc. Int. Symp. Discontinuous Galerkin Methods*, 1999, pp. 425–431.
[30] V. Girault, S. Sun, M. Wheeler, and I. Yotov, "Coupling discontinuous Galerkin and mixed finite element discretizations using mortar finite elements," *SIAM J. Numer. Anal.*, vol. 46, no. 2, pp. 949–979, 2008.
[31] P. R. Devloo, A. M. Farias, S. M. Gomes, and J. L. Gonçalves, "Application of a combined continuous-discontinuous Galerkin finite element method for the solution of the Girkmann problem," *Computers Math. Applic.*, vol. 65, no. 11, pp. 1786–1794, 2013.
[32] I. Perugia and D. Schotzau, "On the coupling of local discontinuous Galerkin and conforming finite element methods," *J. Sci. Computing*, vol. 16, no. 4, pp. 411–433, 2001.
[33] B. Cockburn, J. Gopalakrishnan, and R. Lazarov, "Unified hybridization of discontinuous Galerkin, mixed, continuous Galerkin methods for second order elliptic problems," *SIAM J. Numer. Anal.*, vol. 47, no. 2, pp. 1319–1365, 2009.
[34] A. Cangiani, Geor, and M. Jensen, "Continuous and discontinuous finite element methods for convection-diffusion problems: A comparison," Dept. of Math., Univ. Leicester, Tech. Rep., Jun. 2006.
[35] A. Cangiani, J. Chapman, E. Georgoulis, and M. Jensen, "On the stability of continuous-discontinuous Galerkin methods for advection-diffusion-reaction problems," *J. Sci. Computing*, vol. 57, no. 2, pp. 313–330, 2013.
[36] C. Dawson, J. J. Westerink, J. J. Feyen, J. C. Feyen, and D. Pthina, "Continuous, discontinuous and coupled discontinuous-continuous Galerkin finite element methods for the shallow water equations," *Int. J. Numer. Methods in Fluids*, vol. 52, no. 1, pp. 63–88, 2006.
[37] C. Dawson and J. Proft, "Coupling of continuous and discontinuous Galerkin methods for transport problems," *Comput. Methods in Appl. Mech. Eng.*, vol. 191, no. 29–30, pp. 3213–3231, 2002.
[38] W. Davies, M. K. , and H. O. , "A high order hybrid finite element method applied to the solution of electromagnetic wave scattering problems in the time domain," *Comput. Mech.*, vol. 44, no. 3, pp. 321–331, 2009.
[39] T. Lu, P. Zhang, and W. Cai, "Discontinuous Galerkin methods for dispersive and lossy Maxwell's equations and PML boundary conditions," *J. Computational Phys.*, vol. 200, no. 2, pp. 549–580, 2004.
[40] C.-W. Shu, "Discontinuous Galerkin methods: General approach and stability," in *Numerical Solutions of Partial Differential Equations*, ser. Adv. Courses Math.. Barcelona, Spain: CRM.
[41] J. S. Hesthaven and T. Warburton, "High-order nodal discontinuous Galerkin methods for the Maxwell eigenvalue problem," *Philos. Trans. Royal Soc. London A, Math., Phys. Eng. Sci.*, vol. 362, no. 1816, pp. 493–524, 2004.
[42] M. Ainsworth, "Dispersive and dissipative behaviour of high order discontinuous Galerkin finite element methods," *J. Computational Phys.*, vol. 198, pp. 106–130, Jul. 2004.
[43] J. Alvarez, L. Angulo, M. Fernandez Pantoja, A. Rubio Bretones, and S. Garcia, "Source and boundary implementation in vector and scalar DGTD," *IEEE Trans. Antennas Propag.*, vol. 58, no. 6, pp. 1997–2003, Jun. 2010.
[44] J. Alvarez, J. M. Alonso-Rodriguez, H. Carbajosa-Cobaleda, M. R. Cabello, L. D. Angulo, R. Gomez-Martin, and S. G. Garcia, "DGTD for a class of low-observable targets: A comparison with mom and (2,2) FDTD," *IEEE Antennas Wireless Propag. Lett.*, vol. 13, pp. 241–244, 2014.
[45] A. Bossavit, "Mixed finite elements and the complex of Whitney forms," in *The Mathematics of Finite Elements and Applications, VI (Uxbridge, 1987)*. London, U.K.: Academic, 1988, pp. 137–144.
[46] A. Bossavit, "Whitney forms: A class of finite elements for three-dimensional computations in electromagnetism," *Proc. Inst. Electr. Eng.—Phys. Sci., Meas. Instrum., Manag. Education Rev.*, vol. 135, no. 8, pp. 493–500, 1988.
[47] L. Demkowicz, P. Monk, C. Schwab, and L. Vardapetyan, "Maxwell eigenvalues and discrete compactness in two dimensions," *Comput. Math. Applications*, vol. 40, no. 4–5, pp. 589–605, 2000.
[48] B. He and F. Teixeira, "Differential forms, Galerkin duality, sparse inverse approximations in finite element solutions of Maxwell equations," *IEEE Trans. Antennas Propag.*, vol. 55, no. 5, pp. 1359–1368, May 2007.
[49] D. N. Arnold, R. S. Falk, and R. Winther, "Finite element exterior calculus: From Hodge theory to numerical stability," *Bull. Amer. Math. Soc.*, vol. 47, no. 2, pp. 281–354, 2010.
[50] J. Webb, "Hierarchal vector basis functions of arbitrary order for triangular and tetrahedral finite elements," *IEEE Trans. Antennas Propag.*, vol. 47, no. 8, pp. 1244–1253, Aug. 1999.
[51] G. Mur, "Edge elements, their advantages and their disadvantages," *IEEE Trans. Magn.*, vol. 30, no. 5, pp. 3552–3557, Sep. 1994.
[52] M. Koshiba, K. Hayata, and M. Suzuki, "Vectorial finite-element method without spurious solutions for dielectric waveguide problems," *Electron. Lett.*, vol. 20, no. 1, pp. 409–410, May 1984.
[53] B. Rahman and B. Davies, "Penalty function improvement of waveguide solution by finite elements," *IEEE Trans. Microw. Theory Techn.*, vol. 32, no. 8, pp. 922–928, Aug. 1984.
[54] J. Alvarez, L. D. Angulo, A. Rubio Bretones, and S. Garcia, "A spurious-free discontinuous Galerkin time-domain method for the accurate modeling of microwave filters," *IEEE Trans. Microw. Theory Techn.*, vol. 60, no. 8, pp. 2359–2369, Aug. 2012.
[55] D. Sarmany, M. A. Botchev, and J. J. Vegt, "Dispersion and dissipation error in high-order Runge-Kutta discontinuous Galerkin discretisations of the Maxwell equations," *J. Scientific Computing*, vol. 33, pp. 47–74, Oct. 2007.
[56] H. Moon, F. Teixeira, J. Kim, and Y. Omelchenko, "Trade-offs for unconditional stability in the finite-element time-domain method," *IEEE Microw. Wireless Compon. Lett.*, vol. PP, no. 99, pp. 1–1, 2014.
[57] S. Dosopoulos and J.-F. Lee, "Interconnect and lumped elements modeling in interior penalty discontinuous Galerkin time-domain methods," *J. Comput. Phys.*, vol. 229, no. 22, pp. 8521–8536, 2010.
[58] P. Li and L. J. Jiang, "Integration of arbitrary lumped multiport circuit networks into the discontinuous Galerkin time-domain analysis," *IEEE Trans. Microw. Theory Techn.*, vol. 61, no. 7, pp. 2525–2534, Jul. 2013.
[59] G. Cohen, X. Ferrieres, and S. Pernet, "A spatial high-order hexahedral discontinuous Galerkin method to solve Maxwell's equations in time domain," *Journal of Computational Physics*, vol. 217, no. 2, pp. 340–363, 2006.
[60] J. H. Wilkinson, *The Algebraic Eigenvalue Problem*. Oxford, U.K.: Clarendon, 1964.
[61] C. A. Kennedy, M. H. Carpenter, and R. M. Lewis, "Low-storage, explicit Runge-Kutta schemes for the compressible Navier–Stokes equations," *Appl. Numer. Math.*, vol. 35, pp. 177–219, Nov. 2000.

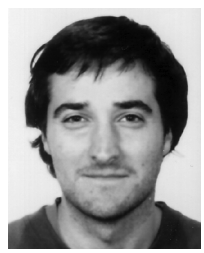

Luis Diaz Angulo was born in Basque Country, Spain, in 1985. He received the B.Sc. and M.Sc. degrees in physics, Ph.D. degree, and M.Sc. degree in electronics engineering from the University of Granada, Granada, Spain, in 2005, 2007, 2014, and 2015, respectively.

He has worked in time-domain numerical methods applied to electromagnetism, especially discontinuous Galerkin time-domain methods and FDTD. Other interests are applications of numerical methods in terahertz technologies, GPR imaging, and bioelectromagnetics.

Jesus Alvarez (M'XX) was born in Leon, Spain. He received the B.Sc. degree from the University of Cantabria, Santander, Spain, in 2001 the M.Sc. degree from the University Carlos III of Madrid, Madrid, Spain, in 2008, and the Ph.D. degree from the University of Granada, Granada, Spain, in 2013.

Since 2006 he has been with Airbus Defence and Space, working as an Antenna and EMC Engineer. His current research interests include computational electrodynamics in time domain, method of moments, and fast algorithms for integral equations in frequency domain and computational electromagnetics applied to electromagnetic compatibility, antenna, and RADAR cross section.

Fernando L. Teixeira (SM'15) received the B.S.E.E. and M.S.E.E. degrees from the Pontifical Catholic University, Rio de Janeiro, Brazil, in 1991 and 1995, respectively, and the Ph.D. degree in electrical engineering from the University of Illinois at Urbana-Champaign, Urbana, IL, USA, in 1999.

From 1999 to 2000, he was a Postdoctoral Associate with the Massachusetts Institute of Technology, Cambridge, MA, USA. In 2000, he joined The Ohio State University, Columbus, OH, USA, where he is now a Professor with the Department of Electrical and Computer Engineering and is affiliated with the ElectroScience Laboratory. His current research interests include modeling of electromagnetic sensors, time-domain computational electromagnetics, metamaterials, and ultra-wideband inverse scattering.

Dr. Teixeira was the recipient of the National Science Foundation CAREER Award, the USNC/URSI triennial Booker Fellowship, and the IEEE Microwave Theory and Techniques Society (MTT-S) Outstanding Young Engineer Award. He has served as chair of the Joint IEEE Antennas and Propagation Society (AP-S)/MTT-S Columbus Chapter and as an associate editor for the IEEE ANTENNAS AND WIRELESS PROPAGATION LETTERS. He currently serves as an associate editor for *IET Microwaves, Antennas and Propagation*.

M. Fernández Pantoja (SM'12) received the B.S., M.S., and Ph.D. degrees from the University of Granada, Granada, Spain, in 1996, 1998, and 2001, respectively, all in electrical engineering.

Between 1997 and 2001, he was an Assistant Professor with the University of Jaen, Spain, and then he joined the University of Granada, Granada, Spain, where, in 2004, he was appointed an Associate Professor. He has been a Guest Researcher with Dipartimento Ingenieria dell'Informazione, University of Pisa, Pisa, Italy, with the Antenna and Electromagnetics Group, Denmark Technical University, and with the CEARL, Pennsylvania State University, State College, PA, USA. His research is focused mainly on the areas of time-domain analysis of electromagnetic radiation and scattering problems, optimization methods applied to antenna design, terahertz technology, and nanoelectromagnetics.

Salvador G. Garcia (SM'14) was born in 1966 in Baeza, Spain. He received the M.S. and Ph.D. degrees (with extraordinary award) from the University of Granada, Granada, Spain, in 1989 and 1994, respectively, both in physics.

In 1999, he joined the Department of Electromagnetism and Matter Physics, University of Granada, Granda, Spain, as an Assistant Professor, and he became a Full Professor in 2012. He has published over 50 refereed journal articles and book chapters and over 80 conference papers and technical reports and has participated in several national and international projects with public and private funding. He has received grants to stay as a Visiting Scholar with the University of Duisburg (1997), the Institute of Mobile and Satellite Communication Techniques (1998), the University of Wisconsin-Madison (2001), and the University of Kentucky (2005). His current research interests include computational electromagnetics, electromagnetic compatibility, terahertz technologies, microwave imaging and sensing (GPR), bioelectromagnetics, and antenna design.